levels during occlusion of the pulmonary artery confirms the diagnosis. Hypoxemia resolves after pneumonectomy. Intratumoral functional shunting should be recognized so that the patient can benefit from surgical treatment.

REFERENCES

1. Pontoppidan H, Geffin B, Lowenstein E. Acute respiratory failure in adults. *N Engl J Med* 1972;287:743–51.
2. Richter Larsen K, Svendsen UG, Milman N, Brenoe J, Petersen BN. Exercise testing in the preoperative evaluation of patients with bronchogenic carcinoma. *Eur Resp J* 1997;10:1559–1565.
3. Carvalho P, Lavender JP. The incidence and etiology of the ventilation–perfusion reverse mismatch defect. *Clin Nucl Med* 1989;14:571–576.
4. Fuentes RT, Holmes RA. Reverse radioaerosol/radioperfusion distribution in pulmonary endobronchial obstruction. *Clin Nucl Med* 1990;15:217–221.
5. Cunningham DA, Lavender JP. Krypton 81m ventilation scanning in chronic obstructive airway disease. *Br J Radiol* 1981;54:110–116.
6. Kao CH. Reverse ventilation/perfusion mismatch. *Semin Nucl Med* 1997;27:183–185.
7. Hawker FH, Torzillo PJ, Southee AE. PEEP and "reverse mismatch." A case where less PEEP is best. *Chest* 1991;99:1034–1036.
8. Kim CK, Heyman S. Ventilation/perfusion mismatch caused by positive pressure ventilatory support. *J Nucl Med* 1989;30:1268–1270.
9. Engeler CE, Kuni CC, Tashjian JH. Regional alterations in lung ventilation in end-stage primary pulmonary hypertension: correlation between CT and scintigraphy. *AJR* 1995;164:831–835.
10. Li DJ, Stewart I, Miles KA, et al. Scintigraphic appearance in patients with pulmonary infection and lung scintigrams of pulmonary embolism. *Clin Nucl Med* 1994;19:1091–1093.
11. Watanabe N, Hirano T, Inoue T, et al. Transient unilateral reverse ventilation/perfusion mismatch in a patient with lung cancer. *Clin Nucl Med* 1992;17:705–708.
12. Shih WJ, Jonston EH, Jonston HW. Reversed abnormal ventilation perfusion scintigraphy in endobronchial squamous cell carcinoma. *Eur J Nucl Med* 1982;7:523–525.
13. Ghetty KG, Dick C, McGovern J, Conroy RM, Mahutte CK. Refractory hypoxemia due to intrapulmonary shunting associated with bronchioalveolar carcinoma. *Chest* 1997;111:1120–1121.
14. Shih WJ, Dillon ML. Matched ventilation-perfusion becomes mismatched ventilation-perfusion lung imaging after resolution of carcinoma of the bronchus. *Clin Nucl Med* 1994;19:279–286.
15. Armas R. Large reverse mismatch associated with pulmonary embolism. *Clin Nucl Med* 1994;19:910–925.
16. Benumof JL, Wahrenbrock EA. Blunted hypoxic pulmonary vasoconstriction by increased lung vascular pressures. *J Appl Physiol* 1975;38:846–850.
17. Spencer RP. Ventilation/perfusion reverse mismatch in septic pulmonary emboli. *Clin Nucl Med* 1996;21:328–329.
18. Kuni CC, Ducret RP, Nakhleh RE, Boudreau RJ. Reverse mismatch between perfusion and aerosol ventilation in transplanted lungs. *Clin Nucl Med* 1993;18:313–317.
19. Slavin JD Jr, Mathews J, Spencer RP. Pulmonary ventilation-perfusion and reverse mismatches in infant. *Clin Nucl Med* 1985;10:708–709.
20. Zucker I, Heyman S, Ozdemir S. Reversed ventilation-perfusion mismatch involving a pediatric patient in congestive heart failure. *J Nucl Med* 1997;38:1681–1683.
21. Sostman HD, Neumann RD, Gottschalk A, Greenspan RH. Perfusion of non ventilated lung: failure of hypoxic vasoconstriction? *AJR* 1983;141:151–156.
22. Levin DP, Pison CF, Brandt M, et al. Reversal of intrapulmonary shunting in cirrhosis after liver transplantation demonstrated by perfusion lung scan. *J Nucl Med* 1991;32:862–864.
23. Suga K, Kuramitsu T, Yoshimizu T, Nakanishi T, Yamada N, Utsmi H. Scintigraphic analysis of hemodynamics in a patient with a single large pulmonary arteriovenous fistula. *Clin Nucl Med* 1992;17:110–113.
24. Simonneau G, Escourou P, Duroux P, Lockart A. Inhibition of hypoxic pulmonary vasoconstriction by nifedipine. *N Engl J Med* 1981;304:1582–1585.
25. McMurtry IF, Davidson AB, Reeves JT, Grover RF. Inhibition of hypoxic pulmonary vasoconstriction by calcium antagonists in isolated rat lungs. *Circ Res* 1976;38:99–104.
26. Perez-Vizcaino F, Villamor E, Moro M, Tamargo J. Pulmonary versus systemic effects of vaodilator drugs: an in vitro study in isolated intrapulmonary and mesenteric arteries of neonatal piglets. *Eur J Pharmacol* 1996;314:91–98.
27. Sakr M, Mikkelsen E. Effects of nifedipine on isolated human pulmonary vessels. *Gen Pharmacol* 1983;14:115–116.
28. Malaisse WJ, Boschero AC. Calcium antagonist and islet function. XI. Effect of nifedipine. *Horm Res* 1977;8:203–209.
29. Kennedy TP, Huang M Jr, Kallman CH, Zahka K, Schlott W, Summer W. Nifedipine inhibits hypoxic pulmonary vasoconstriction during rest and exercise in patients with chronic obstructive pulmonary disease. A controlled double-blind study. *Am Rev Respir Dis* 1984;129:544–551.
30. Wernly JA, DeMeester TR, Kircner PT, Myerowitz PD, Oxford DE, Golomb HM. Clinical value of quantitative ventilation-perfusion lung scans in the surgical management of bronchogenic carcinoma. *J Thorac Cardiovasc Surg* 1980;80:535–543.
31. Markos J, Mullan BP, Hillman DR, et al. Preoperative assessment as a predictor of mortality and morbidity after lung resection. *Am Rev Respir Dis* 1989;13:902–910.

Radiation Absorbed Doses to the Walls of Hollow Organs

James B. Stubbs, Jeffrey F. Evans and Michael G. Stabin

NCO Cath, Inc., Roswell, Georgia; Nuclear Engineering Program, Ohio State University, Columbus, Ohio; and Oak Ridge Institute for Science and Education, Oak Ridge, Tennessee

Many radiopharmacueticals are excreted from the body through the gastrointestinal (GI) tract. The doses to the walls of the organs involved often are very significant. As significant fractions of the administered activity pass through them, these organs may receive the highest doses in the body for many radiopharmaceuticals. The absorbed dose to these walled organs, from activity in their contents, is typically calculated as 50% of the average absorbed dose to the contents, for nonpenetrating emissions. The internal surface of the GI tract, and to a certain extent the urinary bladder, is lined with a variable thickness of mucus. In addition, the radiosensitive cell populations (crypt or stem cells) are located at some depth into the mucosa. These two factors suggest that the surface dose, often used to characterize the clinically relevant absorbed doses for walled organs, may represent an overestimate in some cases. **Methods:** In this study, the radiation transport code MCNP was used to simulate the deposition of energy from nonpenetrating emissions of several radionuclides of interest: ^{90}Y, ^{99m}Tc, ^{123}I and ^{131}I. Absorbed doses as a function of distance from the wall-contents interface were calculated for three geometric shapes representing different organs along the routes of excretion. **Results:** The absorbed dose from nonpenetrating emissions to the sensitive cell populations was consistently lower than estimated by the standard model assumption. The simulated absorbed doses to radiosensitive cells in the GI tract for ^{99m}Tc and ^{123}I are tenfold lower; those for ^{131}I are fivefold lower and those for ^{90}Y are 20% lower. **Conclusion:** This study demonstrates that the normally reported dose to the walls of hollow organs probably should be modified to account for the attenuation of these nonpenetrating emissions in the linings of the walls. This study also demonstrates that Monte Carlo codes continue to be useful in the evaluation of the dose to sensitive cells in walled organs.

Key Words: Monte Carlo; radiation absorbed doses; gastrointestinal tract; electrons; beta particles

J Nucl Med 1998; 39:1989–1995

Received Nov. 20, 1997; revision accepted Feb. 25, 1998.

For correspondence or reprints contact: Michael G. Stabin, PhD, Radiation Internal Dose Information Center, Oak Ridge Institute for Science and Education, P.O. Box 117, Oak Ridge, TN 37831-0117.

Nearly all radiopharmacueticals used in nuclear medicine, both diagnostic and therapeutic, are excreted from the body either through the gastrointestinal (GI) tract or renal system. Because a large fraction of the administered activity usually is excreted through one or both of these routes, the activity in the contents can represent significant sources of radioactivity irradiating the walls of organs in the GI tract or in the urinary bladder.

The absorbed dose to these walled organs, from activity in their contents, has been reported as the absorbed dose to the wall-contents interface. This absorbed dose from the "nonpenetrating" emissions (electrons, beta particles, etc.) typically is estimated as 50% of the average absorbed dose for the contents from the activity in the contents (*1*). The internal surface of the GI tract, and to a certain extent the urinary bladder, is lined with a variable thickness of mucus. In addition, the radiosensitive cell populations (crypt or stem cells) are located at some depth into the mucosa. This study evaluates the appropriateness of the use of this dose at the interface of the walls and contents of hollow organs to characterize the dose to the critical cells within the wall.

Anatomic and Histologic Information

The GI tract is composed of the stomach, gallbladder, small intestine, upper large intestine and lower large intestine. For the renal excretory system, the organ of interest is the urinary bladder. Generally speaking, these organs can be thought of as ellipsoidal or cylindrical shells of tissue surrounding liquid contents. The contents of the proximal GI tract is called chyme; that of the gallbladder, bile; that of the distal GI tract, feces; and that of the urinary bladder, urine. The thicknesses of the walls of these organs are highly variable, ranging from 1–5 mm. Contained within the inner or mucosal layer of the organ walls are the radiosensitive cell populations (crypt or stem cells).

In the GI tract, the cells with appreciable turnover rates, and, thus, radiosensitivity, are found lining either glands (stomach, colon) or the base of villi (small intestine). The average cell lifetime is 4–7 days. The precursor cells (undifferentiated) are found at the base of the glands or crypts. As the precursor cells divide, some daughter cells begin differentiating, specializing in function, and migrating from the crypt region to the mucosal surface or tips of the villi. After reaching these locations, the cells have exhausted their allotted lifetime and, subsequently, slough off into the lumen of the GI tract. When the cells are near the microvilli tips, gland opening or flat absorptive surface, they are at a distance from the lumen contents corresponding to the mucus layer thickness. Under normal physiological conditions, the cells are not in direct contact with the contents.

In the stomach, the mucus layer is about 180 μm thick (*2*), and the surface mucus cells lining the inner surface of the stomach wall are 20–40 μm thick (*3*). The stomach surface is pitted with foveola 200 μm deep by 70 μm in diameter (*3*). At the base of the foveola are the gastric glands that contain radiosensitive cells at a depth of approximately 200 μm (*3*). Thus, the depth to the sensitive cells may be taken as approximately 600 μm.

In the small bowel, the number and height of villi decrease distally toward the terminal region of the ileum. Villi are finger-like structures projecting from the mucosa into the lumen. Few data were found concerning the thickness of the small bowel mucus layer, so a value of 200 μm was used. Small-bowel biopsy of the jejunum, the longest segment of the small intestine, demonstrated mean villus heights of 372 μm and mean crypt depths of 132 μm (*4*). Other investigators have reported mean villus heights of 496 μm (*5*) and 500-1000 μm (*3*), as well as mean crypt depths of 150 μm (*5*). For this study, we used a mucus layer thickness of 200 μm, villus height of 500 μm and crypt depth of 150 μm. Thus, the depth to the sensitive cells may be taken as approximately 850 μm.

The colon has a smooth internal surface pitted with tubular crypts up to 700 μm in depth (*3*). Few data were found concerning the thickness of the small bowel mucus layer, so a value of 200 μm was used. Thus, depth to the sensitive cells, using one-half the crypt depth as where the sensitive cells start being populated, may be taken as approximately 550 μm.

MATERIALS AND METHODS

Models

Three organs were mathematically modeled: the small intestine, the large intestine or colon, and the stomach. The small and large intestines were modeled as cylinders, with an inner cylindrical volume representing the contents and the volume between this cylinder and a second, outer cylinder, representing the intestinal wall. The equations describing the geometry of the intestines are:

$$x^2 + y^2 \geq c^2 \text{ and } x^2 + y^2 \leq (c + 0.5)^2, \qquad \text{Eq. 1}$$

and for the contents,

$$x^2 + y^2 < c^2,$$

$$-5.0 \leq z \leq 5.0. \qquad \text{Eq. 2}$$

The dimensions on all variables are in centimeters. In these equations, c is 1.0 cm and 4.0 cm for the small and large intestines, respectively (*6*). These models represent only isolated segments of the entire intestine. Their representation as upright cylinders of 10 cm in length is arbitrary.

The equations that describe the stomach are taken from the Cristy and Eckerman Reference Adult (*7*) stomach model. The stomach wall is modeled as the volume between two concentric ellipsoids. The stomach contents are modeled as the volume within the inner ellipsoid. The stomach wall is defined by:

$$\left(\frac{x}{4.0}\right)^2 + \left(\frac{y}{3.0}\right)^2 + \left(\frac{z}{8.0}\right)^2 \leq 1.0, \qquad \text{Eq. 3}$$

and

$$\left(\frac{x}{3.387}\right)^2 + \left(\frac{y}{2.387}\right)^2 + \left(\frac{z}{7.387}\right)^2 \geq 1.0, \qquad \text{Eq. 4}$$

and the contents are defined by:

$$\left(\frac{x}{3.387}\right)^2 + \left(\frac{y}{2.387}\right)^2 + \left(\frac{z}{7.387}\right)^2 < 1.0. \qquad \text{Eq. 5}$$

The Monte Carlo computer code, MCNP (*8*), was used to simulate the transport of the beta particles, conversion electrons and Auger electrons from the four radionuclides studied in this work: ^{90}Y, ^{99m}Tc, ^{123}I and ^{131}I. All secondary particles generated from primary interactions, such as knock-on electrons and bremsstrahlung, are simulated by the code.

Radiation Transport Studies

The models for the intestines and the stomach were implemented in MCNP as organs surrounded by a large void space. Energy deposition outside of the organs was not of concern in this study. The composition of the organ wall and contents was assumed to be that of soft tissue, as defined by Cristy and Eckerman (*7*), with a density of 1.04 g/cm^3. Each radionuclide source was assumed to be uniformly distributed within the organ contents.

Emission source spectra for each radionuclide were taken from decay data of Weber et al. (*9*). Iodine-123 decays by electron

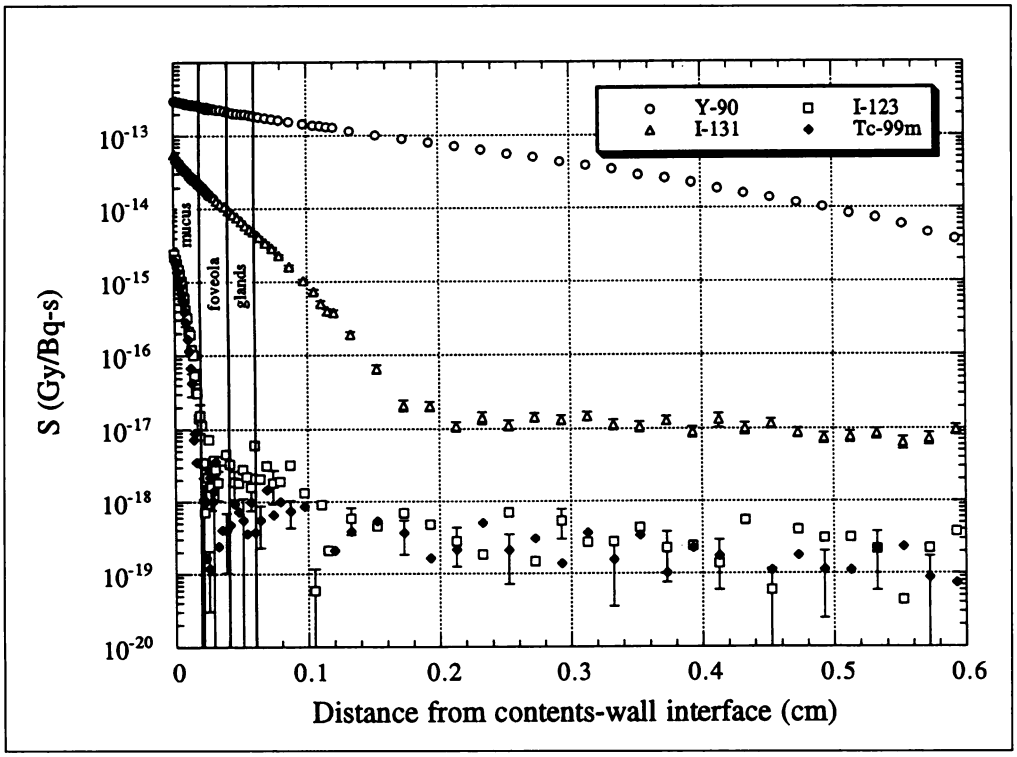

FIGURE 1. Electron dose as function of distance into wall of stomach for all four radionuclides studied.

capture, so its spectrum consists of discrete electron energies from conversion and Auger electrons. Technetium-99m decays almost exclusively by internal conversion (i.e., there is a very low yield of beta emission, so low that its consideration can be neglected entirely), therefore, its spectrum consists entirely of discrete electron energies. Yttrium-90 and ^{131}I both decay by beta emission, hence the spectrum for each consists of a continuous electron energy distribution. The beta spectra for ^{90}Y and ^{131}I were generated from data files and an extraction utility maintained by the Dosimetry Research Group of the Health Sciences Research Division at Oak Ridge National Laboratory (*10*). The ^{131}I spectrum contains five conversion electron energies in conjunction with its beta distribution.

MCNP's energy deposition tally was used to calculate the total energy deposited in the walls of the organs. Tallies were made in concentric shell volumes, which ranged in thickness from 10-μm shells within the inner 300 μm of the wall to 200-μm thick shells through the outer 4000 μm of the wall. The tally results are in units of total energy deposited (MeV) per source particle. These results were converted to units of total energy deposited per decay by multiplying by the number of source particles per decay for each radionuclide. These values then were expressed in the form of mean dose per unit cumulated activity (Gy/Bq-s), through consideration of the energy deposited and the mass of each shell.

The number of particle histories was varied for the different radionuclides to obtain acceptable statistical uncertainties in the reported results. Four million source particle histories were followed for the ^{99m}Tc and ^{123}I calculations, while 3 million histories were followed for the ^{131}I calculations and, approximately, 540,000 histories for the ^{90}Y calculations. The number of electron substeps per energy step was increased to 24 from the default value of 3 for all calculations.

RESULTS

Depth dose distributions were calculated for the three geometries corresponding to the stomach (ellipsoidal; axes 4, 3 and 8 cm), small bowel (cylinder; length 10 cm, radius 1 cm) and large bowel (cylinder; length 10 cm, radius 4 cm). The results for electron dose as a function of distance into the wall in these three geometries for all radionuclides are shown in Figures 1, 2 and 3. Results for photon and electron dose as a function of distance into the wall of the small intestine for ^{131}I, ^{123}I and ^{99m}Tc are shown in Figures 4, 5 and 6.

The absorbed dose to crypt cells in the small bowel from ^{90}Y in the small bowel contents is somewhat less than the standard value of small bowel absorbed dose. For a 1.0-hr residence time, the standard small bowel wall dose would be 0.68 mGy/MBq. The absorbed dose to the small bowel crypt cells, as estimated in this study, is 0.42 mGy/MBq, or about 62% of the standard value.

The relevant, nonpenetrating absorbed dose to the GI tract wall from ^{131}I is less than 10% of the standard value. For ^{123}I and ^{99m}Tc, the absorbed doses to sensitive cells are three orders of magnitude lower than predicted by the standard approach.

The absorbed doses to the sensitive cells also should include the contributions from penetrating emissions, such as the photons of ^{131}I. For ^{131}I, the total S-value at the mucus-contents interface of the small intestine model in this study is 5.5E-13 Gy/Bq-s (5E-14 Gy/Bq-s from photons and 5E-13 Gy/Bq-s from nonpenetrating emissions) (Fig. 4). However, Figure 4 also shows that the total S-value at the surface of the crypt cells is only 7E-14 Gy/Bq-s (5E-14 Gy/Bq-s from photons and 2E-14 Gy/Bq-s from nonpenetrating emissions). Thus, the S-value at the sensitive cell level is only 13% of that at the surface of the contents, even when the photon contributions are included.

For ^{123}I in the same geometry, the calculated total S-value at the mucus-contents interface is 6E-14 Gy/Bq-s (4E-14 Gy/Bq-s from photons and 2E-14 Gy/Bq-s from nonpenetrating emissions) (Fig. 5). However, the total S-value at the crypt-cell level is 3E-14 Gy/Bq-s (3E-14 Gy/Bq-s from photons and <1E-17 Gy/Bq-s from nonpenetrating emissions). Thus, even though the photons contribute significantly to the total S-value at the sensitive cells' depth, the calculated S-value is only 50% of the value normally reported, as the contribution from the nonpenetrating emissions is negligible.

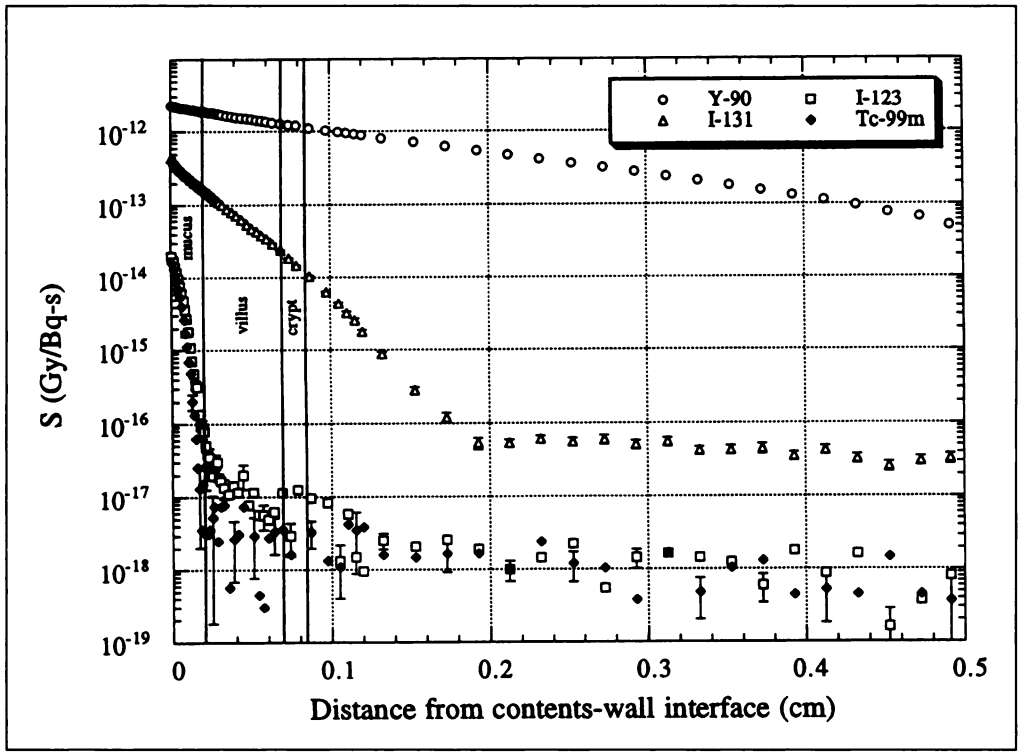

FIGURE 2. Electron dose as function of distance into wall of small intestine for all four radionuclides studied.

For ^{99m}Tc in the same geometry, the total S-value at the mucus-contents interface was 3.6E-14 Gy/Bq-s (1.8E-14 Gy/Bq-s from photons and 1.8E-14 Gy/Bq-s from nonpenetrating emissions) (Fig. 6). The total S-value at the crypt cell level was 1.5E-14 Gy/Bq-s (1.5E-14 Gy/Bq-s from photons and <1E-17 Gy/Bq-s from nonpenetrating emissions). Here, the calculated S-value at the sensitive cell depth is about 42% of the value normally reported.

Table 1 lists the ratio of the electron absorbed dose at the organ content's interface with the mucus layer to the absorbed dose at the location of the sensitive cells (highest point in the crypts, containing radiosensitive cells or cells at significant risk for carcinogenesis). The standard value quoted in internal dosimetry, for so-called "nonpenetrating" emissions (electrons and beta-rays), is the absorbed dose at the contents-mucus interface (i.e., 50% of the dose at the center of the contents).

DISCUSSION

Figure 1 shows the electron (the term "electron" includes all beta particles, conversion and Auger electrons, etc.) dose per

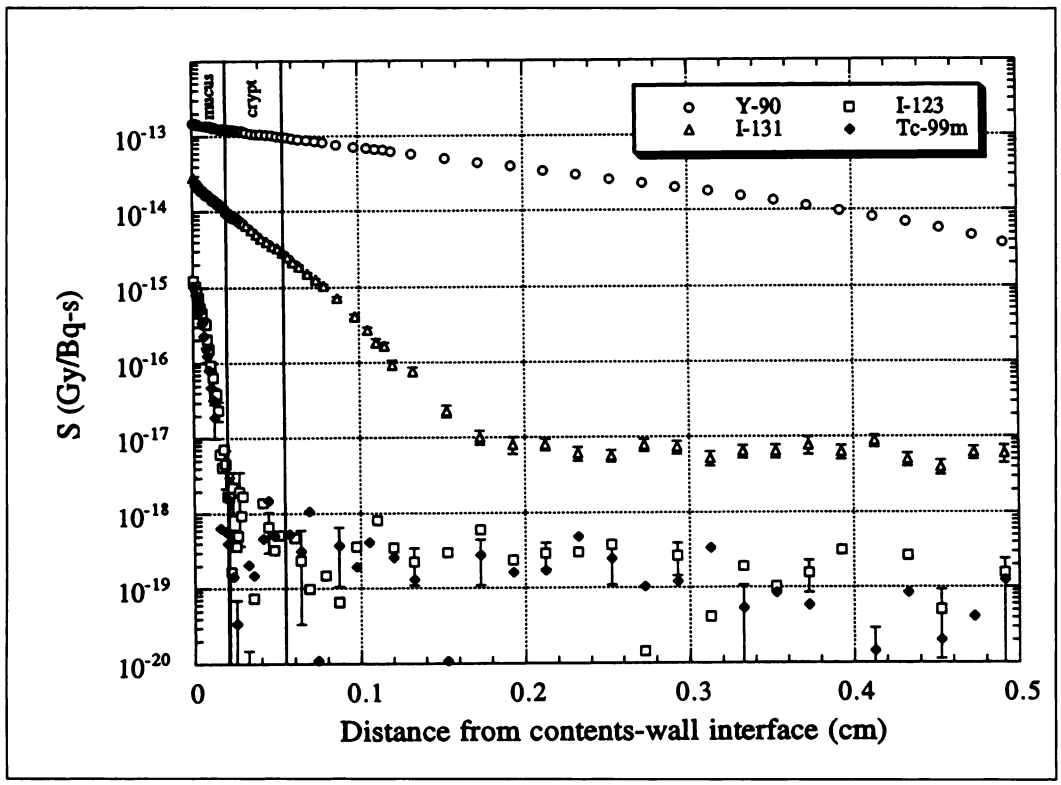

FIGURE 3. Electron dose as function of distance into wall of large intestine for all four radionuclides studied.

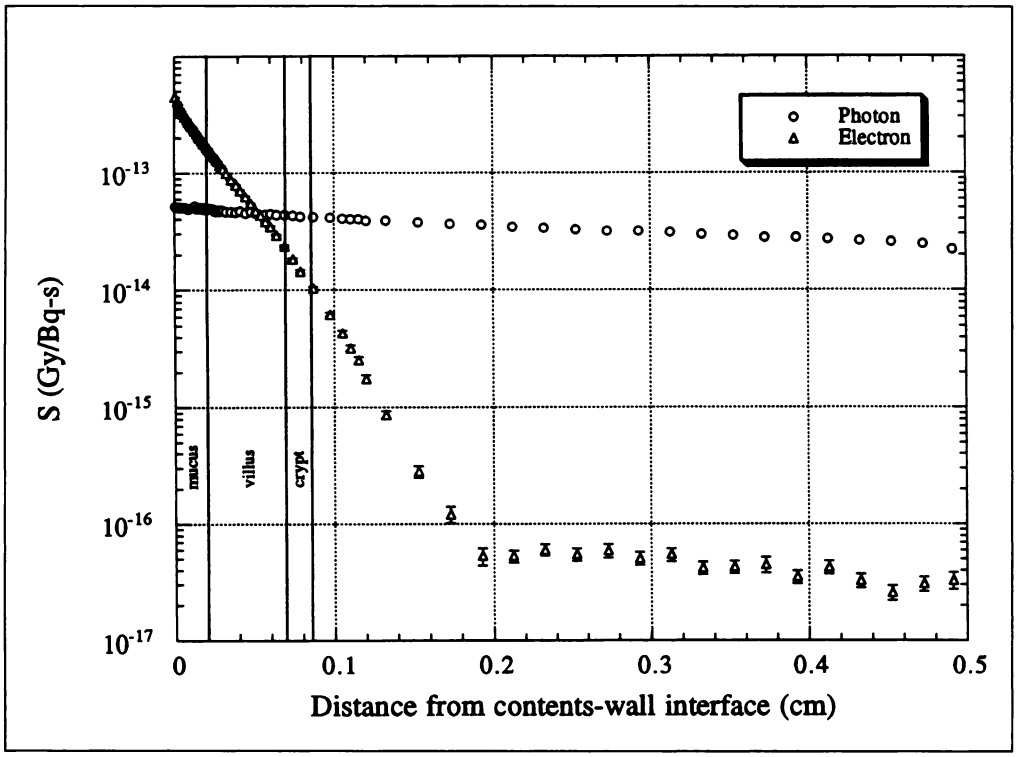

FIGURE 4. Electron and photon dose as function of distance into wall of small intestine for ^{131}I.

disintegration as a function of distance into the wall of the stomach, as modeled in this study. Also shown are approximate depths for the mucus layer, foveola and gland cells. Obviously, these depths are not exactly known and will vary even within a given individual, but they are shown here for reference in interpreting the doses at different distances from the organ contents. For ^{99m}Tc, ^{123}I and ^{131}I, the electron doses drop over several orders of magnitude over the distances studied. The doses estimated on the flatter portion of the curve are contributions from bremsstrahlung radiation (that are associated with more significant uncertainties than are the electron doses, but which are of much smaller magnitude). For ^{90}Y, the beta doses are still significant at 0.6 cm from the source, consistent with the range of these particles in soft tissue (~1 cm). For ^{99m}Tc and ^{123}I, it is clear that the electron doses drop considerably, perhaps to negligible levels before penetrating the mucus layer of the stomach. Even if the mucus layer is somewhat thinner than assumed here, the doses to the foveola and glands are markedly lower than the dose at the interface with the contents. For ^{131}I, the dose has dropped by about a factor of 2 before reaching the foveola and, perhaps, a factor of 5 before reaching the gland cells. Although there is some decrease, the doses from

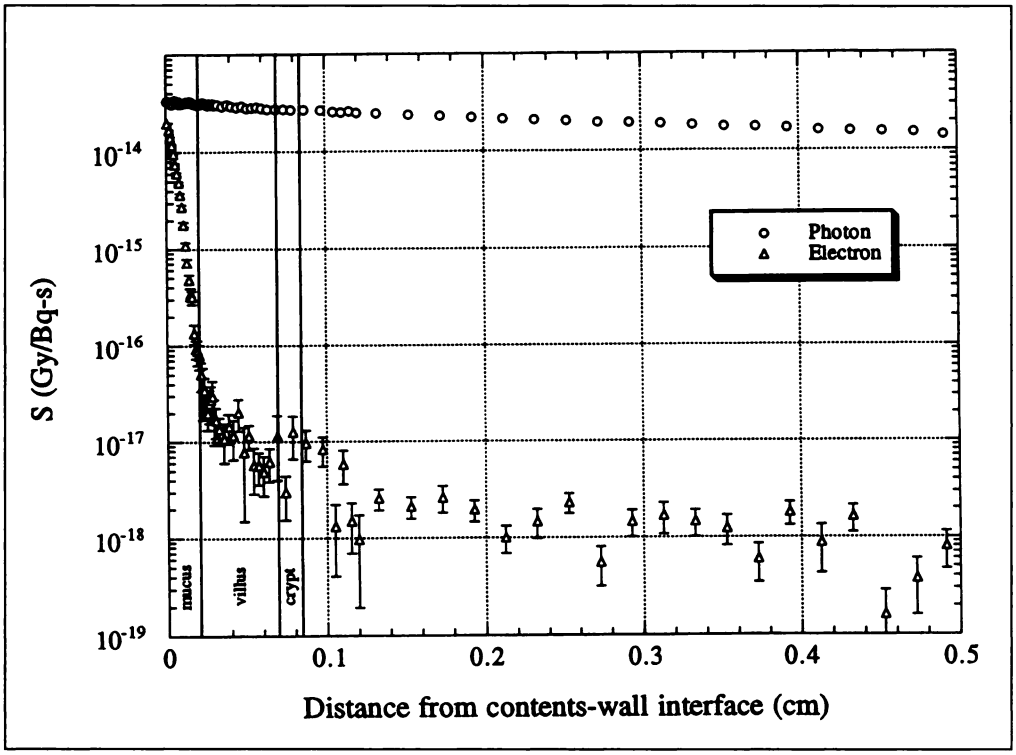

FIGURE 5. Electron and photon dose as function of distance into wall of small intestine for ^{123}I.

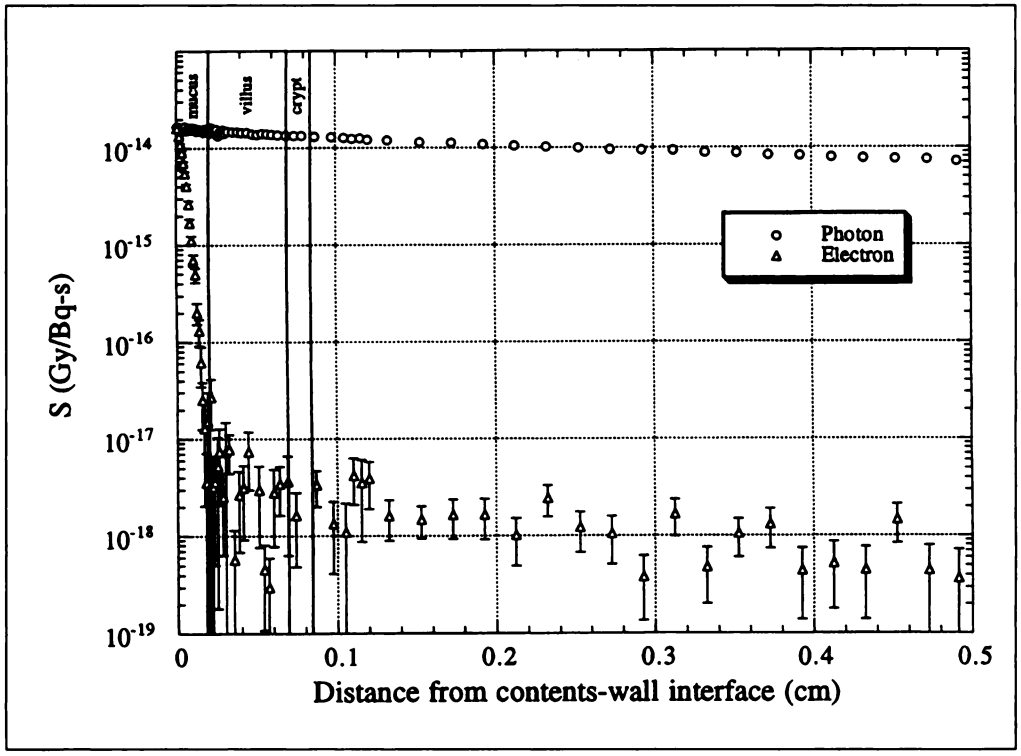

FIGURE 6. Electron and photon dose as function of distance into wall of small intestine for ^{99m}Tc.

^{90}Y have fallen off by not quite a factor of 2 before reaching the glands. In typical dosimetry calculations, the dose right at the interface (distance = 0 in this figure) is used as the dose to the "wall" of this organ. For ^{90}Y, given the uncertainty in the activity concentrations, irradiation geometry, thickness of the mucus lining and other variables, this is probably a reasonable approximation. For ^{99m}Tc and ^{123}I, it is questionable whether any electron dose at all should be assigned to the "wall" of this organ, if the interest is in the dose to the living cells in the wall capable of expressing radiation damage or neoplastic growth. For ^{131}I, it appears that some level of dose should be assigned, but one that is much lower than that at the interface. It is important to remember that this figure shows only the electron doses. The photon dose contribution will be considered later. It is clear that the use of the interface dose to represent the "wall" dose for all radionuclides represents an overestimate of the true dose to biologically important cells, for many radionuclides emitting only moderate- to low-energy electrons.

In the small intestine and colon (Figs. 2 and 3), a similar pattern occurs. In the small intestine (Fig. 2), the ^{90}Y doses have dropped off by perhaps a factor of 2 before reaching the crypt cells, the ^{131}I doses have dropped by more than an order of magnitude, and the ^{99m}Tc and ^{123}I doses have dropped by many orders of magnitude, with only bremsstrahlung contributions remaining. In the colon (Fig. 3), the ^{90}Y doses have dropped slightly before reaching the crypt cells, the ^{131}I doses have dropped by about a factor of 2, and the ^{99m}Tc and ^{123}I doses have dropped markedly.

Figures 4–6 show the relative significance of the photon and electron components of the total self-dose from ^{131}I, ^{123}I and ^{99m}Tc to the wall of the small intestine (it should be recalled that for a photon emitter, other organs in the body may contribute some dose to the total). As expected, the photon doses drop off only slightly over the distances studied, while the electrons drop off as in Figure 2. As noted earlier, the total S values for ^{131}I, ^{123}I and ^{99m}Tc are about 13%, 50% and 42%, respectively, of those at the contents-mucus interface. Thus, the absorbed doses that are reported routinely may in many cases significantly overestimate the dose to the sensitive cells in the intestine wall, as well as in the walls of other hollow organs. Normally, the specific absorbed fraction for a "nonpenetrating" emission originating in the contents and striking the wall is:

$$\Phi = \frac{1.0}{2m_c}, \qquad \text{Eq. 6}$$

where m_c is the mass of the contents of the organ (*1*). The natural solution to this problem is to assign an absorbed fraction of electron energy in the dose calculation, similar to the fraction of 0.01 assigned to alpha emitters by the ICRP (*11*):

TABLE 1
Ratio of Electron Absorbed Dose at Contents-Mucus Interface to Absorbed Dose at Depth of Sensitive Cells

	Stomach	Small bowel		Colon	
Radionuclide	Assumed crypt depth 600 μm	Assumed mucus/villi depth 700 μm	Assumed crypt depth 850 μm	Assumed mucus depth 200 μm	Assumed crypt depth 550 μm
Yttrium-90	6.26E-1	5.61E-1	4.92E-1	8.12E-1	6.56E-1
Iodine-131	8.65E-2	5.29E-2	2.32E-2	3.64E-1	9.93E-2
Iodine-123	1.25E-3	3.46E-4	4.90E-4	2.15E-3	2.14E-4
Technetium-99m	3.14E-4	1.81E-4	1.18E-4	8.06E-4	2.08E-4

$$\Phi = \frac{f_{np}}{2m_c}. \qquad \text{Eq. 7}$$

The choice of a f_{np} (the fraction of the nonpenetrating energy assumed to strike critical cells in the wall) is not straightforward. As mentioned earlier, the actual distances are not completely known, and there will be considerable variability within and between individuals, as there are uncertainties in the actual activity distributions, etc. The values given in Table 1 serve as examples of values that might be applied for the radionuclides specified. A reasonably conservative value could be chosen by a study of this effect across all electron energies and the assignment of values that have a reasonable margin of safety built in. For instance, for a radionuclide that emits only high-energy electrons, such as those from ^{90}Y, the $1/(2m_c)$ model may be maintained. For radionuclides emitting only low-energy conversion or Auger electrons, a very small fraction, say 10^{-4}, or even an absorbed fraction of zero, may be assigned. For intermediate energies, calculations must be done to establish a reasonable function describing the absorbed fraction as a function of energy, given a band of depths expected, and then conservative values may be selected. But clearly, the assignment of a f_{np} of 1.0 to low-energy electrons is overconservative.

The numbers presented in this study are theoretical in nature, as are those based on currently-accepted absorbed fractions. Verification of these numbers through experimental means would further strengthen the conclusions presented, thus providing more confidence in the interpretation of the results, particularly in situations involving therapeutic administrations. Such verification should be pursued in future studies.

CONCLUSION

In this study, the use of the specific absorbed fraction $1/(2m_c)$ to estimate the dose from "nonpenetrating" emissions to the walls of hollow organs was shown to be overly conservative for some radionuclides. Radiation transport studies using the MCNP computer code and relatively simple models of the intestines, stomach and bladder, showed that the actual fraction of electron energy that reaches critical cell layers in the walls of hollow organs may be only a small fraction of that absorbed at the wall-contents interface. For most radionuclides, this latter fraction, which has been traditionally used to characterize the dose to the hollow organs' walls, should be replaced by a similar fraction, one that is modified to take into account that much of the electron energy emitted in the contents may be absorbed in mucus linings or other cell layers before reaching the critical cells.

ACKNOWLEDGMENTS

This work was performed for the U.S. Department of Energy (DOE) under contract DE-AC05-76OR00033 and for the U.S. Food and Drug Administration (FDA) under Interagency Agreement No. FDA 224-75-3016, DOE 40-286-71. This article was written by a contractor of the U.S. Government under contract DE-AC05-76OR00033. Accordingly, the U.S. Government retains a nonexclusive, royalty-free license to publish or reproduce the published form of the contribution, or allow others to do so, for U.S. Government purposes.

The research was performed, in part, under appointment to the Applied Health Physics Fellowship program administered by Oak Ridge Institute for Science and Education for the U.S. DOE.

REFERENCES

1. Snyder W, Ford M, Warner G, Watson S. S, absorbed dose per unit cumulated activity for selected radionuclides and organs. *MIRD Pamphlet No. 11*. New York: Society of Nuclear Medicine; 1975.
2. Allen A. The gastrointestinal system. In: Schultz SG, Forte JG, Rauner BB, eds. *Handbook of physiology (vol. III, section 6)*. Bethesda, MD: American Physiology Society; 1989:359–360.
3. Trier JS, Krone CL, Sleisenger MH. Anatomy, embryology, and developmental abnormalities of the small intestine and colon. In: Sleisenger MH, Fordtran JS, eds. *Gastrointestinal disease–pathophysiology, diagnosis, and management*. Philadelphia: W.B. Saunders Co.; 1983:548, 782.
4. Penna FJ, Hill ID, Kingston D, Robertson K, Slavin G, Shiner M. Jejunal mucosal morphometry in children with and without gut symptoms and normal adults. *J Clin Pathol* 1981;34:386–392.
5. Stenling R, Fredrikzon B, Nyhlin H, Helander HF. Surface ultrastructure of the small intestine mucosa in healthy children and adults: a scanning electron microscopic study with some methodological aspects. *Ultrastruct Pathol* 1984;6:131–140.
6. International Commission on Radiological Protection. *Task group report on reference man*. ICRP Publication 23. Oxford: Pergamon Press; 1975.
7. Cristy M, Eckerman KF. Specific absorbed fractions of energy at various ages from internal photon sources. *ORNL/TM-8381*. Oak Ridge, TN: Oak Ridge National Laboratory; 1987.
8. Briesmeister JF, ed. *MCNP–a general Monte Carlo N-particle transport code–version 4A*. Los Alamos, NM: Los Alamos National Laboratory, LA-12625-M; 1993.
9. Weber DA, Eckerman KF, Dillman LT, Ryman JC. *MIRD: radionuclide data and decay schemes*. New York: The Society of Nuclear Medicine; 1989.
10. Eckerman KF, Westfall RJ, Ryman JC, Cristy M. Availability of nuclear decay data in electronic form, including beta spectra not previously published. *Health Phys* 1994; 67:338–345.
11. International Commission on Radiological Protection. *Limits for intakes of radionuclides by workers*. ICRP Publication 30. New York: Pergamon Press; 1979.